The Astronomical Journal, 153:256 (9pp), 2017 June https://doi.org/10.3847/1538-3881/aa6dfb

A Multi-planet System Transiting the $V = 9$ Rapidly Rotating F-Star HD 106315

Joseph E. Rodriguez, George Zhou, Andrew Vanderburg, Jason D. Eastman, Laura Kreidberg, Phillip A. Cargile, Allyson Bieryla, David W. Latham, Jonathan Irwin, Andrew W. Mayo, Michael L. Calkins, Gilbert A. Esquerdo, and Jessica Mink
Harvard-Smithsonian Center for Astrophysics, 60 Garden Street, Cambridge, MA 02138, USA
Received 2017 January 13; revised 2017 April 18; accepted 2017 April 19; published 2017 May 19

Abstract

We report the discovery of a multi-planet system orbiting HD 106315, a rapidly rotating mid F-type star, using data from the *K2* mission. HD 106315 hosts a $2.51 \pm 0.12\,R_{\oplus}$ sub-Neptune in a 9.5-day orbit and a $4.31^{+0.24}_{-0.27}\,R_{\oplus}$ super-Neptune in a 21-day orbit. The projected rotational velocity of HD 106315 ($12.9\,\mathrm{km\,s^{-1}}$) likely precludes precise measurements of the planets' masses but could enable a measurement of the sky-projected spin–orbit obliquity for the outer planet via Doppler tomography. The eccentricities of both planets were constrained to be consistent with 0, following a global modeling of the system that includes a *Gaia* distance and dynamical arguments. The HD 106315 system is one of few multi-planet systems hosting a Neptune-sized planet for which orbital obliquity measurements are possible, making it an excellent test-case for formation mechanisms of warm-Neptunian systems. The brightness of the host star also makes HD 106315 c a candidate for future transmission spectroscopic follow-up studies.

Key words: planetary systems – planets and satellites: detection – stars: individual (HD 106315)

1. Introduction

The discovery of "hot Jupiters", gas giant planets orbiting very close to their host star, completely changed our understanding of planet formation. While it was once widely believed that Jupiter-mass planets could only form far from their host stars, the discovery of these short-period massive planets demonstrated that planet formation and migration is a far more complex and dynamic process than previously thought. Theories for the origins of hot Jupiters include the idea that they form farther out in the protoplanetary disk, and through various mechanisms, migrate inward. However, the large number of compact planetary systems with Neptune-sized objects discovered in the last decade have led to the idea that smaller gaseous planets in close-in orbits might form in situ (Chiang & Laughlin 2013; Boley et al. 2016) and that hot Jupiters might form this way as well (Batygin et al. 2016). Lee et al. (2014) showed that runaway accretion of hydrogen gas around rocky cores can occur in the inner disk (0.1 au), leading to planets with significant gaseous envelopes. Huang et al. (2016) found that giant planets outward of 10-day period orbits are preferentially found in multi-planet systems, as opposed to the population of typically lonely hot Jupiters and hot Neptunes. This suggests that hot Jupiters might have migrated inward chaotically, disrupting any inner planetary systems, while warm Neptunes perhaps formed in situ, often within compact planetary systems.

Tracers for the formation mechanisms of these planetary systems lie in their present-day orbital configurations, so characterizable transiting systems are key for us to discern the origins of these warm-Neptune/super-Earth systems. Hansen & Murray (2013) proposed that compact super-Earth systems that formed in situ should exhibit small non-zero eccentricity distributions. Measuring the angle between the orbital angular momentum vector and the host star's rotational axis—its obliquity angle—provides another major observational clue as to the way planets form and migrate. Lonely planets in high-obliquity orbits could have been dynamically injected inward by outer companions (e.g., HAT-P-11 b, Hirano et al. 2011; Sanchis-Ojeda & Winn 2011) while co-planar high-obliquity planetary systems (e.g., *Kepler*-56, Huber et al. 2013) may have formed within a torqued disk that was excited through interactions with stellar companions or magnetic fields (Batygin 2012; Spalding & Batygin 2014). Such torquing and warping of circumstellar disks around young stars has been well documented with high-resolution imaging by the *Hubble Space Telescope* (Beta Pictoris, Kalas & Jewitt 1995; Heap et al. 2000) and by the millimeter mapping with the Atacama Large Millimeter/submillimeter Array (HD 142527, Marino et al. 2015).

Recently, measurements of the Rossiter–McLaughlin effect (McLaughlin 1924; Rossiter 1924) and Doppler tomography (Collier Cameron et al. 2010) for transiting hot Jupiters have revealed a pattern that planet orbits and host star spins tend to be well aligned for cool stars and misaligned for hot stars (Winn et al. 2010; Albrecht et al. 2012). The change from aligned systems to misaligned systems appears to happen at a $T_{\rm eff} \sim 6250$ K, where there is a known transition between slowly and rapidly rotating stars, referred to as the Kraft break (Kraft 1967, 1970). It is believed that the lack of a convection zone in rapidly rotating stars above the Kraft break allows them to conserve more angular momentum from formation and have weaker magnetic fields, resulting in less magnetic braking from stellar wind (van Saders & Pinsonneault 2013). Similarly, observations of young disk-bearing T Tauri and Herbig Ae/Be stars have shown that the magnetic field strength decreases with stellar mass (Gregory et al. 2012; Alecian et al. 2013). Albrecht et al. (2012) suggest that this trend in spin/orbit misalignments could be the signature of planet–planet scattering bringing hot Jupiters close into their host stars on highly eccentric orbits, where the stronger tidal interactions with stars having a convective zone below the Kraft break bring the envelopes of cool stars back into alignment with the planetary orbits. However, Mazeh et al. (2015) and Li & Winn (2016) used photometric spot modulation of *Kepler* systems to show that this trend continues for smaller planets in longer-period orbits, where tidal and magnetic interactions are significantly weaker and realignment of the stellar envelope is unlikely. Precise

spectroscopic obliquity measurements of smaller-radius or longer-period planetary systems around hot stars are key to solving this problem.

Few planetary systems with small- or long-period planets transiting hot stars are amenable to such detailed characterization to discern their origins. Ground-based transit surveys are mostly sensitive to Jupiter-sized objects with short orbital periods, and while NASA's *Kepler* mission has found many systems of small- and long-period planets, most of the host stars are too faint for follow-up observations. The *K2* mission and the upcoming *Transiting Exoplanet Survey Satellite* (*TESS*) mission (Ricker et al. 2015) offer opportunities to find small planets transiting bright stars above/below the Kraft break by virtue of looking at many more bright stars than the *Kepler* mission did. *K2* has yielded over 100 planet discoveries, many of which orbit bright stars (Crossfield et al. 2016; Sinukoff et al. 2016; Vanderburg et al. 2016b), and *TESS* is expected to find over 1000 planets transiting the closest and brightest stars in the sky (Sullivan et al. 2015). By virtue of their high photometric precision and wide-field survey designs, these missions will discover small planets transiting hot stars amenable to spectroscopic measurements of obliquity.

In this paper, we present the discovery of two transiting planets orbiting the bright, $V = 9$ star HD 106315 (Table 1) from the *K2* mission. The close-in planet, HD 106315 b is a $2.5 \pm 0.1\,R_\oplus$ sub-Neptune on a $9.5539^{+0.0009}_{-0.0007}$ day period, while the outer planet, HD 106315 c, is a $4.3^{+0.2}_{-0.3}\,R_\oplus$ super-Neptune in a 21.058 ± 0.002 day period. The host star has a temperature above the Kraft break and, as such, is rapidly rotating at a projected speed of $12.9 \pm 0.4\,\mathrm{km\,s^{-1}}$. The rapid rotation, brightness of the host star, and depth of the outer planet's transit make Doppler Tomography observations to determine the spin–orbit misalignment of the HD 106315 system possible with high-resolution spectrographs on moderate aperture telescopes. HD 106315 c could be the first warm Neptune-sized planet orbiting a star above the Kraft break with a measured spin–orbit angle, providing crucial information to its formation and evolutionary history.

Table 1
HD 106315 Magnitudes and Kinematics

Other Identifiers	HD 106315 TYC 4940-868-1 EPIC 201437844 2MASS J12135339-0023365		
Parameter	Description	Value	References
α_{J2000}	Right Ascension (R.A.)	12:13:53.394	(1)
δ_{J2000}	Declination (decl.)	−00:23:36.54	(1)
B_T	Tycho B_T mag.	9.488 ± 0.022	(1)
V_T	Tycho V_T mag.	9.004 ± 0.018	(1)
J	2MASS J mag.	8.116 ± 0.026	(2), (3)
H	2MASS H mag.	7.962 ± 0.040	(2), (3)
K_S	2MASS K_S mag.	7.853 ± 0.020	(2), (3)
WISE1	*WISE1* mag.	7.805 ± 0.023	(4), (5)
WISE2	*WISE2* mag.	7.857 ± 0.019	(4), (5)
WISE3	*WISE3* mag.	7.856 ± 0.023	(4), (5)
WISE4	*WISE4* mag.	7.898 ± 0.246	(4), (5)
μ_α	*Gaia* DR1 proper motion in R.A. (mas yr^{-1})	-1.678 ± 0.636	(6)
μ_δ	*Gaia* DR1 proper motion in decl. (mas yr^{-1})	11.912 ± 0.460	(6)
RV	Systemic radial velocity (km s^{-1})	-3.65 ± 0.1	Section 2.2
$v \sin i_\star$	Rotational velocity	12.9 ± 0.4 km s^{-1}	Section 2.2
$[m/\mathrm{H}]$	Metallicity	-0.27 ± 0.08	Section 2.2
$T_{\rm eff}$	Effective Temperature	6251 ± 52 K	Section 2.2
$\log(g)$	Surface Gravity	4.1 ± 0.1 (cgs)	Section 2.2
$V_{\rm mac}$	Macroturbulent Velocity	4.0 ± 0.3 km s^{-1}	Section 2.2
$V_{\rm mic}$ (fixed)	Microturbulent Velocity	1.9 km s^{-1}	Section 2.2
d	Distance (pc)	107.3 ± 3.9	(6)
Spec. Type	Spectral Type	F5V	(7)

Note. References are: (1) Høg et al. (2000), (2) Cutri et al. (2003), (3) Skrutskie et al. (2006), (4) Wright et al. (2010), (5) Cutri et al. (2014), (6) Gaia Collaboration et al. (2016) *Gaia* DR1 http://gea.esac.esa.int/archive/, (7) Houk & Swift (1999).

2. Observations

2.1. K2 Photometry

After the failure of its second fine-pointing reaction wheel, the *Kepler* spacecraft has been re-purposed to obtain highly precise photometric observations of a set of fields near the ecliptic for its extended *K2* mission (Howell et al. 2014). As part of *K2* Campaign 10, the *Kepler* telescope observed HD 106315 between 2016 July 6 and September 20. Usually, *K2* observes targets continuously for 80 days at a time, but during Campaign 10, the spacecraft suffered several unanticipated anomalies. During the first six days of the campaign (2016 July 6–13), the the spacecraft's pointing was off by about 12 arcsec, causing many targets to fall at least partially outside of their "postage stamp" apertures. The pointing was then corrected, and *Kepler* observed for about seven more days until one of the spacecraft's CCD modules failed on 2016 July 20. The module failure caused *Kepler* to go into safe mode, and data collection was halted until 2016 August 3, at which point data collection proceeded normally until the end of the campaign on 2016 September 20. Upon public release of the *K2* campaign 10 data set, we downloaded the target pixel files, produced light curves, corrected for *Kepler*'s unstable pointing precision and known systematics using the technique described in Vanderburg & Johnson (2014), and searched for transiting planets with the pipeline described by Vanderburg et al. (2016c). Our transit search identified two transiting planet candidates orbiting HD 106315: a candidate super-Neptune in a 21-day orbit, and a candidate sub-Neptune in a 9.5-day orbit. We then re-processed the *K2* light curve by removing 4σ upward outliers and the two largest single-point downward outliers, and simultaneously fitting the transit signals, *K2* systematics, and long-term flux variations using the method described by Vanderburg et al. (2016c). For our analysis, we only use the data collected after the pointing correction on 2016 July 13, a total of 2506 data points taken over the course of 69 days (see Figure 1). We flattened the light curves for modeling by dividing away the best-fit low-frequency variations (which we modeled as a basis spline with breakpoints every 0.75 days) from our simultaneously fit re-processed light curve.

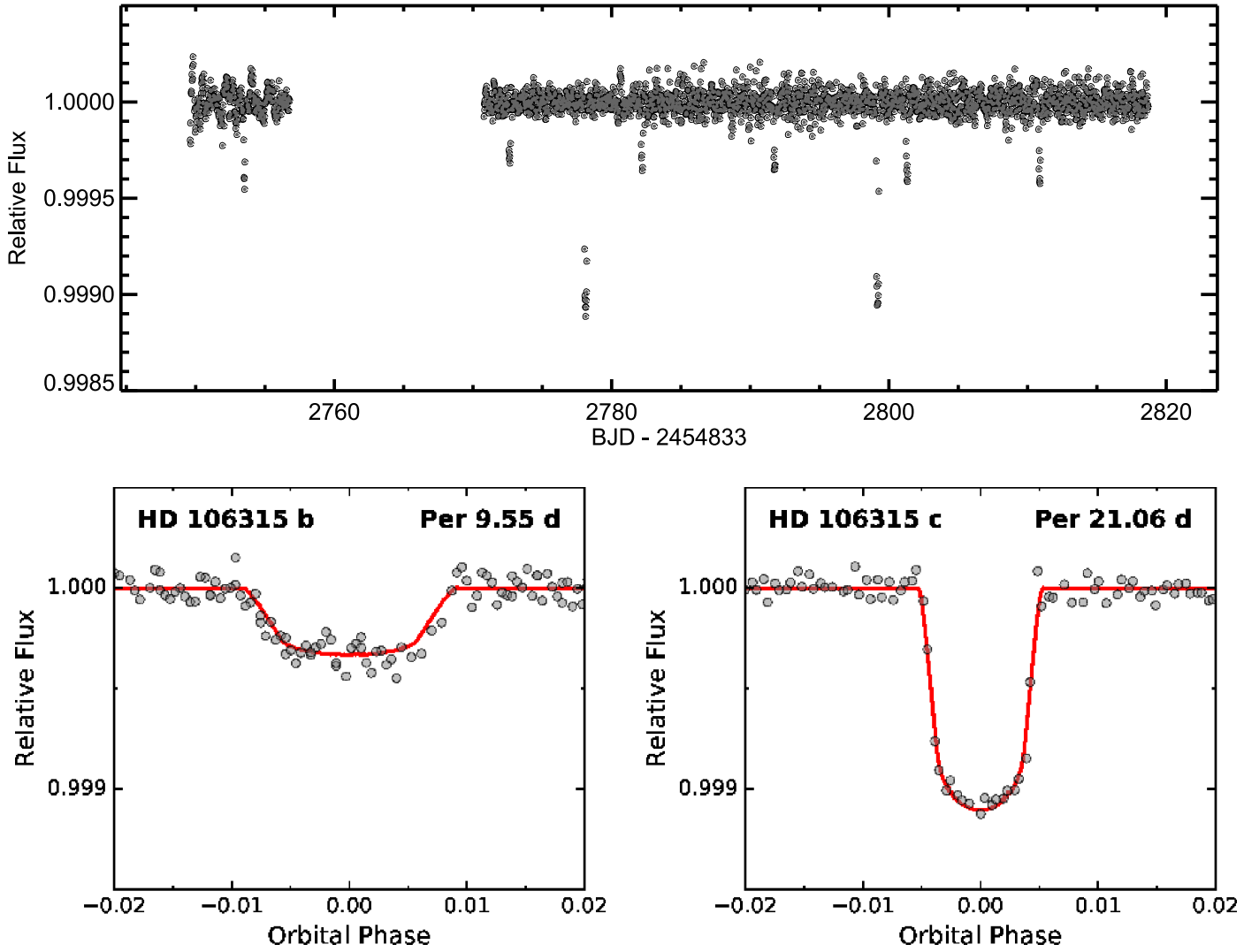

Figure 1. Top panel: the corrected *K2* light curve for HD 106315 using the technique described in Vanderburg & Johnson (2014). Bottom panel: phase folded *K2* light curves of HD 106315 b and c. The observations are plotted in gray, and the best-fit model is plotted in red.

2.2. Tillinghast Reflector Echelle Spectrograph (TRES) Spectroscopy

To measure the spectroscopic parameters of HD 106315, we used the TRES on the 1.5 m telescope at the Fred L. Whipple Observatory (FLWO) on Mt. Hopkins, AZ. TRES is a fiber-fed echelle spectrograph, with a spectral resolving power of $\lambda/\Delta\lambda = 44{,}000$. We observed HD 106315 twice: on UT 2016 December 26 we obtained a 150 s exposure with a signal-to-noise ratio (S/N) per resolution element of 41.7 at over the peak of the Mg b line order, and on UT 2017 January 8 we obtained a 990 s exposure, yielding an S/N of 122. After cross-correlating the stellar spectra with synthetic templates, we find no evidence of a second set of spectral lines or any sign of a nearby blended source. The radial velocities measured from the two spectra differ by only 66 m s^{-1}, consistent with the expected RV uncertainties. After applying a correction to place the velocity of HD 106315 on the IAU standard system, we measure an absolute RV of -3.65 ± 0.1 km s^{-1}. From the stronger spectrum, we measured the star's Mt. Wilson activity indices $S_{\rm HK} = 0.166 \pm 0.004$ and $\log R'_{\rm HK} = -4.90 \pm 0.02$. Our measurements of the Mt. Wilson activity indicators were calibrated by comparing activity measurements from TRES observations of stars also observed in the Mt. Wilson survey by Duncan et al. (1991).

Using the Stellar Parameter Classification (SPC) tool, we inferred that HD 106315 has a $T_{\rm eff} = 6251 \pm 52$ K, $[m/{\rm H}] = -0.27 \pm 0.08$, $\log(g) = 4.1 \pm 0.1$ (cgs), and a projected rotational velocity of 14.6 ± 0.5 km s^{-1} (Buchhave et al. 2012, 2014). SPC determines these parameters by cross-correlating the observed stellar spectra with a grid of synthetic spectra from Kurucz (1992). The synthetic spectra used by SPC includes a microturbulent velocity of 1.9 km s^{-1}. SPC does not model macroturbulence, so we also independently derived $v \sin I_\star$ and the macroturbulent velocity from least-squares deconvolution line profiles, derived from the TRES spectra (Collier Cameron et al. 2010, following). We fit the least-squares deconvolution broadening profiles simultaneously with the parameters $v \sin I_\star$ and the macroturbulent velocity, finding values of $v \sin I_\star = 12.9 \pm 0.4$ km s^{-1} and $v_{\rm mac}$ of 4.0 ± 0.3 km s^{-1}. This is consistent with the macroturbulence of late F-stars measured by Doyle et al. (2014), which were determined by spectroscopic follow-up of a series of *Kepler* astro-seismic stars. We note that these errors are likely underestimated, as they do not include any systematic problems that may be present in the fitting or the LSD derivation.

2.3. Archival and Seeing-limited Imaging

To rule out the possibility of nearby bright companions, we visually inspected archival *J*-band observations of HD 106315 from the 3.8 m United Kingdom Infrared Telescope (UKIRT) located on Mauna Kea. We also observed HD 106315 with KeplerCam on the 1.2 m telescope at FLWO. KeplerCam has a $23' \times 23'$ field-of-view and is binned 2×2 resulting in a $0\farcs67$ pixel scale. Additionally, we observed HD 106315 with one of the eight MEarth-South telescopes. MEarth-South is located at the Cerro Tololo Inter-American Observatory in Chile and consists of eight 0.4 m telescopes, each with a $29' \times 29'$ field-of-view and a $0\farcs85$ pixel scale. From the combined archival and seeing-limited images, we confidently rule out any bright companions to HD 106315 outside of about an arcsecond and rule out any other stars inside the *K2* photometric aperture at larger distances.

3. System Modeling

3.1. Spectral Energy Distribution and Stellar Properties

To determine the stellar properties of HD 106315, we model all available photometry using MINES*weeper* (P. A. Cargile et al. 2017, in preparation). MINES*weeper* is a newly developed Bayesian approach for determining stellar parameters using the newest MIST stellar evolution models (Choi et al. 2016). A detailed description of MINES*weeper* is given in P. A. Cargile et al. (2017, in preparation), and a brief summary can be seen in Section 4 of Rodriguez et al. (2017). Unlike the case of V1334 Tau (Rodriguez et al. 2017), we use the SPC spectral results[1] ([Fe/H], $T_{\rm eff}$, and Log(g); see Section 2.2) and *Gaia* TGAS parallax measurements as priors in our analysis (Gaia Collaboration et al. 2016). We excluded the APASS photometry from this analysis due to our past experience with unaccounted for zero-point offsets (P. A. Cargile et al. 2017, in preparation). Our final SED model is shown in Figure 2. The determined stellar parameters are: Stellar Age $= 3.987^{+0.802}_{-0.516}$ Gyr, $M_\star = 1.105^{+0.028}_{-0.036}\,M_\odot$, $R_\star = 1.286^{+0.039}_{-0.040}\,R_\odot$, $\log(L_\star) = 0.368^{+0.028}_{-0.026}\,L_\odot$, $T_{\rm eff} = 6300 \pm 37$ K, $\log(g) = 4.261^{+0.027}_{-0.024}$ cgs, $[{\rm Fe/H}]_{\rm initial} = -0.128^{+0.041}_{-0.065}$ (metallicity at formation), $[{\rm Fe/H}]_{\rm surface} = -0.268^{+0.060}_{-0.071}$ (current stellar metallicity), Distance $= 109 \pm 3$ Pc, and $Av = 0.005^{+0.027}_{-0.001}$ mag. This analysis used the MIST stellar evolution models, while our global analysis used the YY Isochrones or the Dartmouth stellar evolution models. We use this analysis to check the global model determined stellar parameters (Section 3.2). Additionally, the SED analysis shows no sign of any IR excess and is consistent with a $T_{\rm eff} = 6300$ K stellar photosphere.

3.2. Global Model

We make use of the flattened *K2* light curves, *Gaia* parallax, and TRES spectroscopic stellar parameters to perform a global modeling of the HD 106315 system. Two independent analyses are presented in Table 2, incorporating the Dartmouth (Dotter et al. 2008) and YY (Yi et al. 2001) isochrones. The systematic errors between the different stellar models used in the global model and Section 3.1 are the likely cause of the

[1] Note: While SPC measures metallicity ($[m/{\rm H}]$), (that is, holding abundance ratios fixed at solar values and only adjusting the overall metal content), throughout our analysis, we use $[m/{\rm H}]$ and [Fe/H] interchangeably.

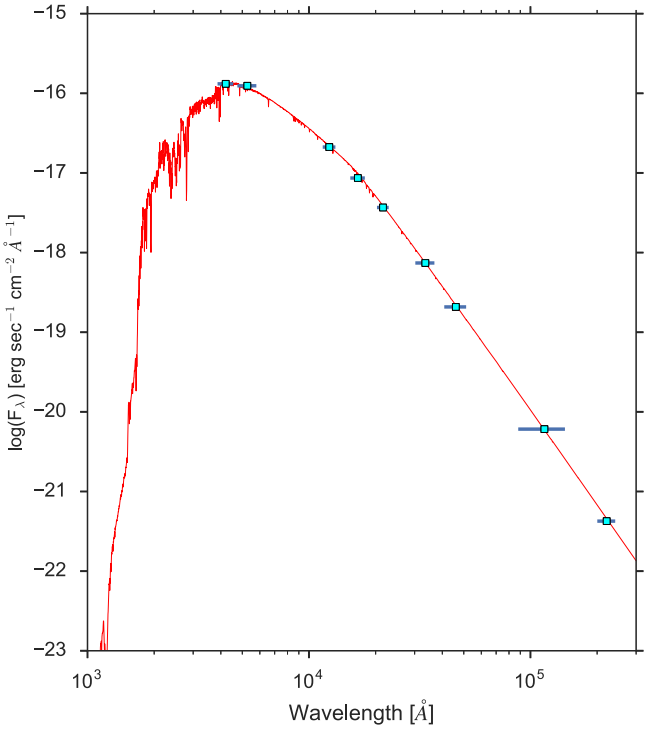

Figure 2. Spectral energy distribution of HD 106315 with a model using the inferred stellar parameters from MINES*weeper*. The light blue points show the Tycho-2 B_T, V_T, 2MASS *J*, *H*, K_s, and *WISE*1–4 photometric observations included in the fit. The red curve represents the best-fit MIST stellar model.

$\sim 1.5\sigma$ discrepancy in age and $\sim 2\sigma$ difference in stellar mass. We note that the stellar radius between all stellar models is consistent (see Table 2).

The Dartmouth models are incorporated in a global analysis (labeled "Dartmouth" in Table 2), with the light curves modeled using a modified version of *EBOP* (Nelson & Davis 1972; Popper & Etzel 1981; Southworth et al. 2004). The models are determined by the transit parameters of each planet: transit centroids T_0, periods P, radius ratios $R_p/R_\star$, normalized orbital radii $a/R_\star$, orbit inclination i, and eccentricity parameters $\sqrt{e}\cos\omega$ and $\sqrt{e}\sin\omega$. The quadratic limb darkening coefficients are fixed to those interpolated as per Sing (2010). In addition, we incorporate the effective temperature $T_{\rm eff}$ and metallicity ($[M/{\rm H}]$) with tight Gaussian priors into our analysis. At each iteration, we calculate a stellar density $\rho_\star$ from the transit parameters, as per Seager & Mallén-Ornelas (2003) and Sozzetti et al. (2007), and fit these stellar parameters to the Dartmouth isochrones (Dotter et al. 2008) to derive a distance modulus. The distance modulus is then compared with the *Gaia* parallax via a likelihood penalty, further constraining the stellar and transit parameters.

The parameter space is explored via a Markov chain Monte Carlo (MCMC) exercise, using the *emcee* affine invariant ensemble sampler (Foreman-Mackey et al. 2013). To avoid dynamically unstable solutions, links of the MCMC chain where the two orbits cross the Hill sphere of HD 106315 b are removed. To calculate the Hill radius, we estimate the mass of each planet via mass–radius relationships from Weiss & Marcy (2014, $R_p < 4\,R_\oplus$) and Lissauer et al. (2011, $R_p > 4\,R_\oplus$). The resulting Hill spheres of b and c are small (0.002 au), such that this constraint is essentially the removal of orbital crossing solutions in the MCMC chain. We also restrict the solutions such that the surface of HD 106315 b does not extend beyond

Table 2
HD 106315 System Parameters

Parameter	Description	Dartmouth Adopted Value	YY Value
Stellar parameters			
$M_\star(M_\odot)$	Stellar mass	$1.027^{+0.034}_{-0.029}$	$1.086^{+0.042}_{-0.044}$
$R_\star(R_\odot)$	Stellar radius	$1.281^{+0.051}_{-0.058}$	$1.308^{+0.054}_{-0.050}$
$T_{\rm eff}$ (K)[a]	Effective temperature	6254^{+55}_{-51}	6248^{+48}_{-47}
log $g_\star$	Surface gravity	$4.234^{+0.035}_{-0.033}$	4.240 ± 0.036
$[M/{\rm H}]$[b]	Metallicity	$-0.278^{+0.082}_{-0.073}$	$-0.279^{+0.076}_{-0.074}$
Age (Gyr)	Age	$5.91^{+0.90}_{-0.79}$	$4.68^{+1.1}_{-0.94}$
$L_\star(L_\odot)$	Luminosity	$2.24^{+0.18}_{-0.16}$	$2.34^{+0.18}_{-0.16}$
Distance (pc)	Distance	$109.7^{+4.2}_{-4.4}$	$107.5^{+3.9}_{-3.6}$
Planet b			
P (d)	Orbital period	$9.55385^{+0.00095}_{-0.00072}$	$9.55496^{+0.00091}_{-0.00096}$
T_0 ($\rm BJD_{TDB}$)	Transit centroid timing	247615.2057 ± 0.0017	$2457615.2063^{+0.0015}_{-0.0016}$
$R_p(R_\oplus)$	Planet radius	2.40 ± 0.12	$2.56^{+0.14}_{-0.13}$
$R_p(R_{\rm J})$	Planet radius	0.214 ± 0.011	$0.228^{+0.013}_{-0.012}$
$R_p/R_\star$	Radius ratio	$0.01717^{+0.00069}_{-0.00055}$	$0.01792^{+0.00054}_{-0.00053}$
$a/R_\star$	Normalized orbital radius	$14.86^{+0.64}_{-0.52}$	$15.00^{+0.60}_{-0.58}$
$i(^\circ)$	Orbit inclination	$87.62^{+1.59}_{-0.44}$	$87.61^{+0.97}_{-0.34}$
b	Impact parameter	$0.63^{+0.08}_{-0.43}$	$0.59^{+0.11}_{-0.31}$
a (au)	Orbital distance	$0.08887^{+0.00082}_{-0.00093}$	0.0912 ± 0.0012
e	Eccentricity	$<0.31(1\sigma)$[c]	$0.25(1\sigma)$[c]
$\omega(^\circ)$	Argument of periastron	67^{+72}_{-134}	89^{+84}_{-85}
$T_{\rm eq}$ (K)	Equilibrium temperature	1146^{+19}_{-22}	1140 ± 20
T_{14} (days)	Total duration	$0.159^{+0.041}_{-0.009}$	$0.1548^{+0.0036}_{-0.0035}$
τ (days)	Ingress/egress duration	$0.00444^{+0.00082}_{-0.00089}$	0.0042 ± 0.0013
T_S ($\rm BJD_{TDB}$)	Time of occultation	2457610.6 ± 1.1	$2457619.99^{+0.94}_{-0.93}$
Planet c			
P (d)	Orbital period	$21.0580^{+0.0022}_{-0.0022}$	21.0575 ± 0.0014
T_0 ($\rm BJD_{TDB}$)	Transit centroid timing	$2457611.1328^{+0.0015}_{-0.0014}$	$2457611.13263^{+0.00097}_{-0.00099}$
$R_p(R_\oplus)$	Planet radius	$4.40^{+0.25}_{-0.27}$	$4.50^{+0.24}_{-0.22}$
$R_p(R_{\rm J})$	Planet radius	$0.393^{+0.022}_{-0.024}$	$0.401^{+0.021}_{-0.020}$
$R_p/R_\star$	Radius ratio	$0.03207^{+0.0009}_{-0.0011}$	$0.03159^{+0.00075}_{-0.00085}$
$a/R_\star$	Normalized orbital radius	$25.69^{+1.2}_{-1.1}$	$25.70^{+1.0}_{-0.98}$
inc $(^\circ)$	Transit inclination	$88.48^{+0.19}_{-0.18}$	$88.51^{+0.39}_{-0.18}$
b	Impact parameter	$0.688^{+0.044}_{-0.094}$	$0.61^{+0.11}_{-0.23}$
a (au)	Orbital distance	$0.1503^{+0.0015}_{-0.0015}$	$0.1564^{+0.0021}_{-0.0022}$
e	Eccentricity	$<0.18(1\sigma)$[c]	$<0.23(1\sigma)$[c]
$\omega(^\circ)$	Argument of periastron	53^{+77}_{-134}	89 ± 61
$T_{\rm eq}$ (K)	Equilibrium temperature	874^{+18}_{-19}	871 ± 15
T_{14} (days)	Total duration (days)	$0.1970^{+0.0035}_{-0.0027}$	$0.1939^{+0.0029}_{-0.0028}$
τ (days)	Ingress/egress duration	0.0115 ± 0.0017	$0.0092^{+0.0028}_{-0.0026}$
T_S ($\rm BJD_{TDB}$)	Time of eclipse	$2457600.55^{+0.49}_{-0.69}$	2457600.6 ± 1.6

Notes.
[a] $T_{\rm eff}$ is constrained by a Gaussian prior about its spectroscopically determined parameters.
[b] $[M/{\rm H}]$ is constrained by a Gaussian prior about its spectroscopically determined parameters.
[c] Solutions with Hill sphere crossings have been removed.

its Roche lobe at periastron (following Hartman et al. 2011). Because the radius of HD 106315 b is small, this is a also weak constraint that only removes the highest eccentricity solutions for this system. The best-fit results are presented in Table 2 and Figure 1, and the derived eccentricity posteriors for each planet are shown in Figure 3.

We also model the HD 106315 system via the new EXOFASTv2 code (labeled "YY" in Table 2). EXOFASTv2 (J. D. Eastman et al. 2017, in preparation) is based on EXOFAST (Eastman et al. 2013), but many of the high-level codes were re-written from the ground up to be more general and flexible, allowing us to fit multiple planets, multiple sources of radial velocities, multiple transits with non-periodic transit times, different normalizations, or separate band passes with just command line options and configuration files. It is also far easier to add additional effects and parameters.

EXOFASTv2 retains the global consistency of the model star and planet that the previous version had, but with the ability to

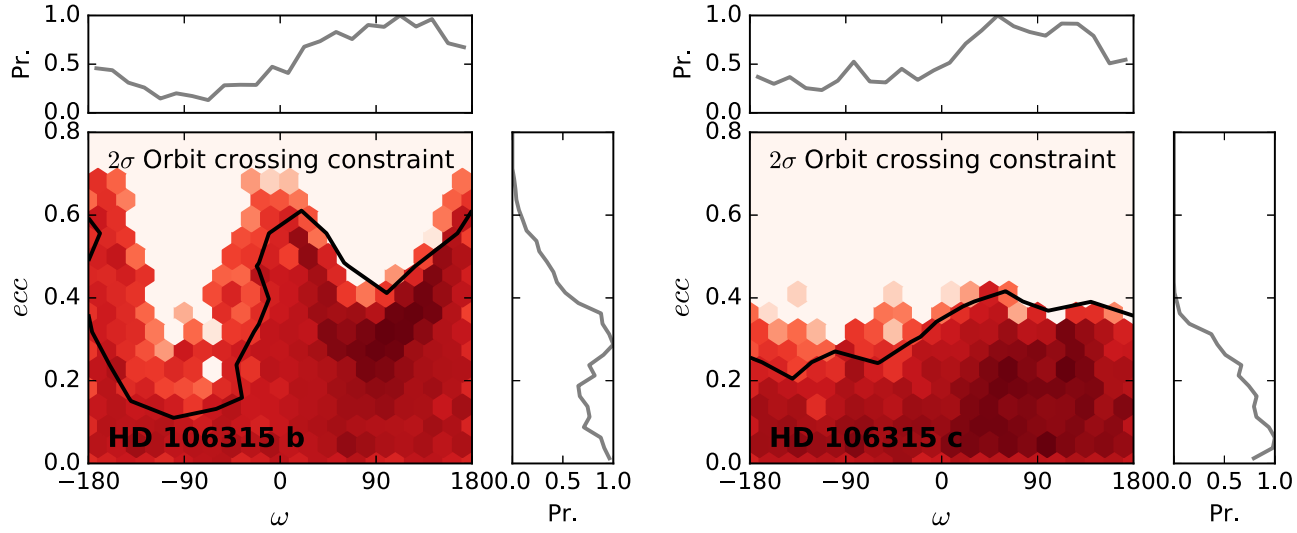

Figure 3. Eccentricity (ecc) and argument of periastron (ω) posterior probability distributions for HD 106315 b (left) and c (right). The contours mark the regimes where 95% of the solutions lie for the MCMC chains constrained by the orbit crossing criteria. In addition, the side panels mark the marginalized posteriors for eccentricity and ω.

fit multiple planets, and we now apply additional global constraints, like requiring that each planet's transit model implies the same stellar density (Seager & Mallén-Ornelas 2003) and their orbits are stable (i.e., they do not cross into other planets' Hill Spheres). Similar to the way EXOFAST handles limb darkening coefficients, EXOFASTv2 imposes a Gaussian prior derived from the Claret & Bloemen (2011) quadratic limb darkening tables, given each step's value for the $\log(g)$, $T_{\rm eff}$, and [Fe/H], assuming model uncertainties of 0.05 in each limb darkening parameter.

The major conceptual departures from the original EXOFAST are that we use Yonsei–Yale isochrones (Yi et al. 2001) to simultaneously model the star instead of the Torres relations (Torres et al. 2010; see Eastman et al. 2016 for a more detailed description), we replace the stepping parameter $\log g$ with age, for which uniform priors should be more physical, and we replace the stepping parameter $\log(a/R_*)$ with $\log(M_*)$, which allows for a more straight-forward extension to multiple planets, as the semimajor axis is trivially derived from M_* and the period using Kepler's law. We also now fit an added variance term instead of scaling and fixing the uncertainties.

The two major conceptual departures from the independent analysis above are that we use the YY stellar models instead of Dartmouth and we use the Chen & Kipping (2017) exoplanet mass–radius relation (instead of Weiss & Marcy 2014 and Lissauer et al. 2011) to estimate the planetary masses in order to exclude planetary eccentricities that would drive them into each other's Hill spheres.

We have used this system to validate EXOFASTv2 and fully characterize the system. We include spectroscopic priors from the SPC analysis on $\log g$, $T_{\rm eff}$, and [Fe/H]. The results of the EXOFASTv2 fit can be seen in Table 2. All determined values for the YY and Dartmouth separate global fits are consistent with each other to $\sim 1\sigma$. We present both the Dartmouth and YY results in Table 2. While we have no reason to prefer one over the other, for concreteness, we adopt the Dartmouth global model results for our discussion. The eccentricity of both planets is consistent with the orbits (circular) with limits of <0.30 for planet b and <0.066 for planet c at 95% confidence.

4. Statistical Validation

Occasionally, transit signals like the ones we see in the *K2* light curve of HD 106315 can be caused by astrophysical phenomena other than transiting planets. We calculated the probability of such scenarios for the HD 106315 planet candidates using `vespa` (Morton 2015), an implementation of the statistical procedure described by Morton (2012) to determine the likelihood that a transit signal is caused by a *bona fide* exoplanet. `Vespa` calculates false positive probabilities for transiting planet candidates using information about the shape of the transits, constraints on the presence of other nearby stars, the location of the star in the sky (and, hence, the likelihood of an undetected background star contaminating the light curve), constraints in the difference in transit depth between even and odd transits, and constraints on the depth of putative secondary eclipses. `Vespa` considers several false positive scenarios, including the possibility that the transit signals are due to foreground eclipsing binary stars. For HD 106315, we include the additional constraint, as we rule out an eclipsing binary scenario by our two different TRES observations that show no significant radial velocity difference.

With `vespa`, we calculate false positive probabilities of 5×10^{-3} and 3×10^{-6} for HD 106315 b and c, respectively. Because HD 106315 hosts multiple transiting planet candidates, it is even less likely that the candidates transiting HD 106315 are false positives. Lissauer et al. (2012) calculated a "multiplicity boost," or decrease in false positive probability for multi-transiting systems in the *Kepler* field of about a factor of 25. Subsequently, Sinukoff et al. (2016) and Vanderburg et al. (2016c) have calculated that the multiplicity boost for *K2* candidates is similar in magnitude. Applying the multiplicity boost to the HD 106315 planets decreases the false positive probabilities to 2×10^{-4} and 10^{-7} for HD 106315 b and c, respectively. Therefore, we conclude that HD 106315 b and HD 106315 c are validated as genuine exoplanets.

5. Discussion

The HD 106315 system stands out among the currently known population of transiting planets for several reasons.

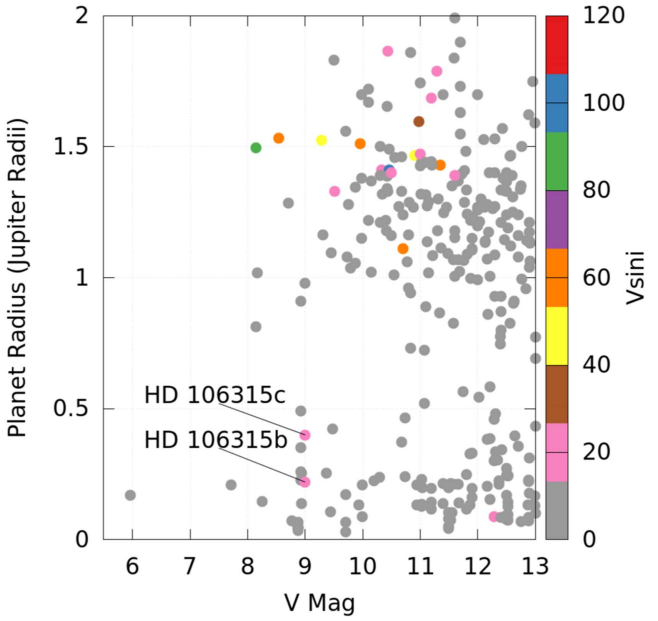

Figure 4. Measured planet radii for all confirmed transiting planets brighter than $V = 13.0$, color-coded by $v \sin I_*$. This figure was created using Filtergraph (Burger et al. 2013).

First, HD 106315 is one of the brightest host stars to host sub-Jovian planets. We accessed the NASA Exoplanet Archive (Akeson et al. 2013) on 2017 January 11 and found only eight stars hosting planets smaller than $0.5\,R_J$ that are brighter than HD 106315. Of these bright sub-Jovian hosts, HD 106315 is the only star above the Kraft break with a rotational velocity greater than $10\,\mathrm{km\,s^{-1}}$. While ground-based transit surveys have found giant planets around hot rapidly rotating bright stars (Collier Cameron et al. 2010; Hartman et al. 2015; Zhou et al. 2016), the HD 106315 system is the first example of a multi-transiting system of small planets orbiting this type of star. Figure 4 shows the HD 106315 system in the context of other transiting planet systems. The brightness, small planet radii, and fast rotation make the HD 106315 planets attractive targets for follow-up observations.

5.1. Prospects for Doppler Tomography

The large numbers of compact Neptune/super-Earth systems discovered by the primary *Kepler* mission have prompted the renaissance of in situ formation models for planets with gaseous envelopes (Lee et al. 2014; Batygin et al. 2016; Boley et al. 2016). The formation and migrational history of planetary systems are embedded in their present-day orbital obliquities. However, few multi-planet systems offer the opportunity for us to characterize their orbital obliquities via unbiased techniques. The obliquities of multi-planetary systems and longer-period warm Jupiters can be measured via star-spot crossings (e.g., Sanchis-Ojeda et al. 2012; Dai & Winn 2017), and via asteroseismology for planets around evolved stars (e.g., Huber et al. 2013; Quinn et al. 2015). Figure 5 (left panel) shows the set of planets for which obliquities have been measured spectroscopically.[2] WASP-47 is the only multi-transiting system with a spectroscopically measured obliquity (Becker et al. 2015; Sanchis-Ojeda et al. 2015).

[2] From the Holt–Rossiter–McLaughlin Encyclopedia http://www2.mps.mpg.de/homes/heller/.

The possibility of further obliquity characterization for the HD 106315 system makes this discovery especially important. HD 106315 is a $V = 9.0$ star with a $v \sin I_*$ of $12.9\,\mathrm{km\,s^{-1}}$, making it an excellent target for further follow-up via Doppler tomography (e.g., Collier Cameron et al. 2010; Johnson et al. 2014; Zhou et al. 2016). Figure 5 (right panel) shows a simulated Doppler tomographic transit of HD 106315 b, as observed by the Magellan Inamori Kyocera Echelle (MIKE) spectrograph on the 6.5 m *Magellan* Clay telescope. We assume an exposure time of 15 minutes, each with an S/N scaled from that of the TRES spectra presented in Section 2.2 and spectral resolution convolved to that of MIKE ($\lambda/\Delta\lambda = 65{,}000$). A macroturbulence broadening of $4\,\mathrm{km\,s^{-1}}$ has also been included, accounting for additional broadening of the line profiles. The planetary Doppler tomography signal is detected at a significance of 7σ.

5.2. Prospects for Transmission Spectroscopy

Transmission spectroscopy will also be a powerful diagnostic of the system's formation history. The planets' atmospheric compositions depend on their origin. For example, a planet forming outside of the water ice line can accrete water-rich planetesimals, whereas we would expect closer-in formation locations to lead to a drier composition (Chiang & Laughlin 2013).

HD 106315 stands out as a prime system for atmosphere characterization thanks to the brightness of the host star (H mag $= 8$). As shown in Table 3, both planets rank in the top twenty best small planets for transmission spectroscopy measurements ($R_P < 5\,R_\oplus$). The S/N calculations were made with the same assumptions in Vanderburg et al. (2016b).

Although they are among the highest S/N candidates known, the HD 106315 planets still pose a challenge for transmission spectroscopy with current facilities. To assess prospects for observing the system with *HST*/WFC3, the current state-of-the-art instrument for atmosphere studies, we calculated a model spectrum for the outer planet with the ExoTransmit code (Kempton et al. 2016). We assumed a 100× solar metallicity atmosphere and a surface gravity equal to $7\,\mathrm{m\,s^{-2}}$ ($M_P = 15\,M_\oplus$). For this case, the amplitude of spectral features is just 70 ppm, which is within reach of an intensive multi-transit observing campaign with *HST* (e.g., Kreidberg et al. 2014; Line et al. 2016). However, if the planet mass is larger, the atmosphere is more enhanced in metals, or aerosols are present, the amplitude of spectral features will decrease, and they may not be detectable until *JWST* launches.

A further complication is that the planet masses are unknown and will be challenging to measure. HD 106315 is a rapid rotator ($v \sin I_* = 12.9\,\mathrm{km\,s^{-1}}$), which broadens the lines and inhibits precise RV measurements. According to the NASA Exoplanet Archive (accessed 2017 January 10), for all planet-hosting stars with a $v \sin I_* > 10\,\mathrm{km\,s^{-1}}$, the smallest measured RV semi-amplitude is $33\,\mathrm{m\,s^{-1}}$, whereas the expected semi-amplitude for HD 106315 c is only 2–5 $\mathrm{m\,s^{-1}}$. The absence of mass measurements is problematic for interpreting the transmission spectrum, because atmospheric metallicity and surface gravity are highly degenerate (Batalha et al. 2017). Therefore, to take full advantage of the potential this system has for precise transmission spectroscopy, it will be necessary to explore alternative prospects for measuring the masses. Recently, progress has been made measuring the masses of small planets around moderately rotating stars using advanced statistical techniques and high-cadence observations (see, for

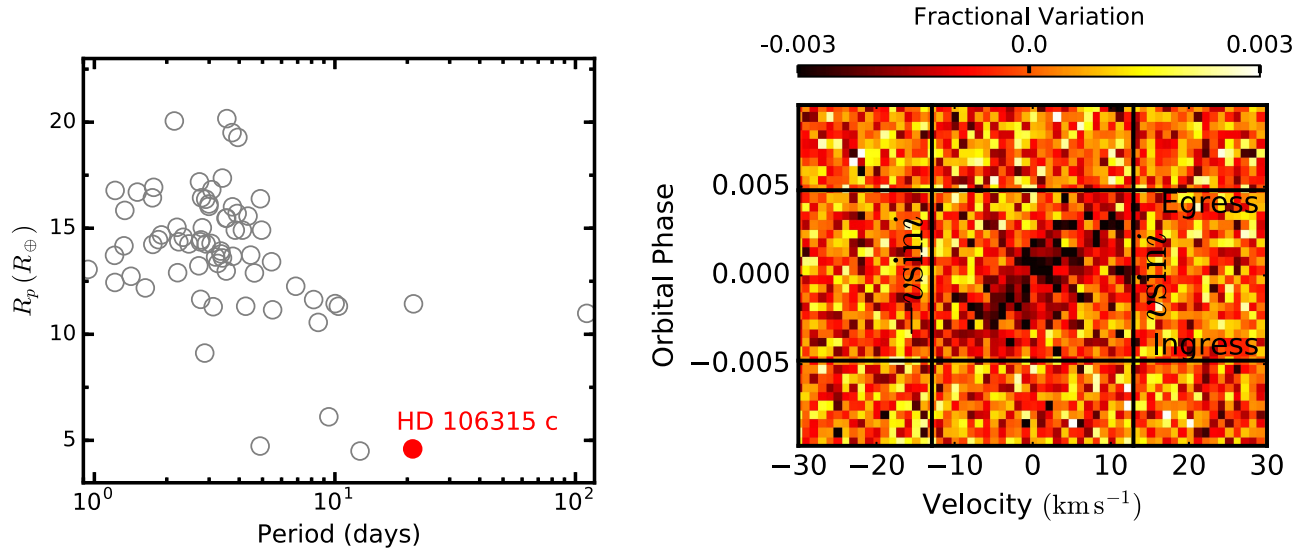

Figure 5. Left panel: period–planet radius distribution for all planets with secure spectroscopic obliquities measured. HD 106315 c would be one of the longest period, smallest planets for which an obliquity can be measured. Right panel: simulated Doppler tomographic detection signal from observing a single transit of HD 106315 c using the MIKE. The ingress and egress are represented by the horizontal black lines, and the boundaries of $-v \sin I_*$ and $v \sin I_*$ are marked by the vertical back lines.

Table 3
The Best Confirmed Planets for Transmission Spectroscopy with $R_P < 5\,R_\oplus$

Planet	$R_P(R_\oplus)$	S/N[a]	Reference
GJ 1214 b	2.85 ± 0.20	1.00	Charbonneau et al. (2009)
GJ 436 b	4.1697408	0.68	Gillon et al. (2007)
GJ 3470 b	3.88 ± 0.33	0.48	Bonfils et al. (2012)
HAT-P-11 b	4.73 ± 0.26	0.46	Bakos et al. (2010)
55 Cnc e	1.91 ± 0.08	0.41	Dawson & Fabrycky (2010)
HD 97658 b	$2.34^{+0.17}_{-0.15}$	0.30	Dragomir et al. (2013)
HD 3167 c	$2.85^{+0.24}_{-0.15}$	0.26	Vanderburg et al. (2016b)
HD 106315 c	$4.3^{+0.2}_{-0.3}$	0.22	This work
K2-25 b	$3.43^{+0.95}_{-0.31}$	0.22	Mann et al. (2016)
HIP 41378 d	3.96 ± 0.59	0.19	Vanderburg et al. (2016a)
HIP 41378 b	2.90 ± 0.44	0.14	Vanderburg et al. (2016a)
K2-32 d	3.76 ± 0.40	0.13	Dai et al. (2016)
K2-19 c	$4.86^{+0.62}_{-0.44}$	0.12	Armstrong et al. (2015)
K2-28 b	2.32 ± 0.24	0.12	Hirano et al. (2016)
K2-32 c	$3.48^{+0.98}_{-0.42}$	0.12	Dai et al. (2016)
Kepler-105 b	4.81 ± 1.5	0.11	Wang et al. (2014)
Kepler-411 c	$3.27^{+0.12}_{-0.067}$	0.11	Morton et al. (2016)
HD 106315 b	2.5 ± 0.1	0.10	This work

Note.
[a] The predicted signal-to-noise ratios relative to GJ 1214 b.

example, López-Morales et al. 2016), but measuring the masses of the HD 106315 planets will be an even greater challenge. Transit timing variations (TTVs) could be an alternate way to measure planet masses, but HD 106315 b and c do not orbit particularly close to any strong mean motion resonances ($P_C/P_B \simeq 2.2$), so any TTVs will be small.

6. Conclusion

We present the discovery of two transiting planets orbiting the bright F-star HD 106315. HD 106315 b is a sub-Neptune size planet with a radius of $2.5 \pm 0.1\,R_\oplus$ and a $9.5539^{+0.0009}_{-0.0007}$ day orbit. HD 106315 c is a warm super-Neptune size planet with a radius of $4.3^{+0.2}_{-0.3}\,R_\oplus$ and an orbital period of 21.058 ± 0.002 days. The large rotational velocity of HD 106315 provides an attractive opportunity to measure the spin–orbit angle for a Neptune-sized planet. This measurement may provide evidence to distinguish whether HD 106315 c formed in situ or farther out in the protoplanetary disk and migrated to its current location. Future observations should attempt to measure the mass of each planet, a parameter important for proper interpretation of any transit spectroscopy, but such mass determinations will likely require capabilities beyond what is presently achievable with precise RV measurements or TTVs.

Work performed by J.E.R. was supported by the Harvard Future Faculty Leaders Postdoctoral fellowship. A.V. is supported by the NSF Graduate Research Fellowship, grant No. DGE 1144152. D.W.L. acknowledges partial support from the from the *TESS* mission through a sub-award from the Massachusetts Institute of Technology to the Smithsonian Astrophysical Observatory. Work performed by P.A.C. was supported by NASA grant NNX13AI46G. This research has made use of NASA's Astrophysics Data System and the NASA Exoplanet Archive, which is operated by the California Institute of Technology, under contract with the National Aeronautics and Space Administration under the Exoplanet Exploration Program. This paper includes data collected by the *Kepler* mission. Funding for the *K2* mission is provided by the NASA Science Mission directorate. Some of the data presented in this paper were obtained from the Mikulski Archive for Space Telescopes (MAST). STScI is operated by the Association of Universities for Research in Astronomy, Inc., under NASA contract NAS5-26555. Support for MAST for non-*HST* data is provided by the NASA Office of Space Science via grant NNX13AC07G and by other grants and contracts. UKIRT is supported by NASA and operated under an agreement among the University of Hawaii, the University of Arizona, and Lockheed Martin Advanced Technology Center; operations are enabled through the cooperation of the East Asian Observatory.

Note added in review. During the preparation of this paper, our team became aware of another paper reporting the discovery of a planetary

system orbiting HD 106315 (Crossfield et al. 2017). The results from both papers are consistent with each other. No information about the analysis procedure or any results were shared between groups prior to the submission of both papers.

References

Akeson, R. L., Chen, X., Ciardi, D., et al. 2013, PASP, 125, 989
Albrecht, S., Winn, J. N., Johnson, J. A., et al. 2012, ApJ, 757, 18
Alecian, E., Wade, G. A., Catala, C., et al. 2013, MNRAS, 429, 1001
Armstrong, D. J., Santerne, A., Veras, D., et al. 2015, A&A, 582, A33
Bakos, G. Á, Torres, G., Pál, A., et al. 2010, ApJ, 710, 1724
Batalha, N. E., Kempton, E. M.-R., & Mbarek, R. 2017, arXiv:1701.00012
Batygin, K. 2012, Natur, 491, 418
Batygin, K., Bodenheimer, P. H., & Laughlin, G. P. 2016, ApJ, 829, 114
Becker, J. C., Vanderburg, A., Adams, F. C., Rappaport, S. A., & Schwengeler, H. M. 2015, ApJL, 812, L18
Boley, A. C., Granados Contreras, A. P., & Gladman, B. 2016, ApJL, 817, L17
Bonfils, X., Gillon, M., Udry, S., et al. 2012, A&A, 546, A27
Buchhave, L. A., Bizzarro, M., Latham, D. W., et al. 2014, Natur, 509, 593
Buchhave, L. A., Latham, D. W., Johansen, A., et al. 2012, Natur, 486, 375
Burger, D., Stassun, K. G., Pepper, J., et al. 2013, A&C, 2, 40
Charbonneau, D., Berta, Z. K., Irwin, J., et al. 2009, Natur, 462, 891
Chen, J., & Kipping, D. 2017, ApJ, 834, 17
Chiang, E., & Laughlin, G. 2013, MNRAS, 431, 3444
Choi, J., Dotter, A., Conroy, C., et al. 2016, arXiv:1604.08592
Claret, A., & Bloemen, S. 2011, A&A, 529, A75
Collier Cameron, A., Guenther, E., Smalley, B., et al. 2010, MNRAS, 407, 507
Crossfield, I. J. M., Ciardi, D. R., Isaacson, H., et al. 2017, arXiv:1701.03811
Crossfield, I. J. M., Ciardi, D. R., Petigura, E. A., et al. 2016, ApJS, 226, 7
Cutri, R. M., Skrutskie, M. F., van Dyk, S., et al. 2003, yCat, 2246, 0
Cutri, R. M., et al. 2014, yCat, 2328, 0
Dai, F., & Winn, J. N. 2017, arXiv:1702.04734
Dai, F., Winn, J. N., Albrecht, S., et al. 2016, ApJ, 823, 115
Dawson, R. I., & Fabrycky, D. C. 2010, ApJ, 722, 937
Dotter, A., Chaboyer, B., Jevremović, D., et al. 2008, ApJS, 178, 89
Doyle, A. P., Davies, G. R., Smalley, B., Chaplin, W. J., & Elsworth, Y. 2014, MNRAS, 444, 3592
Dragomir, D., Matthews, J. M., Eastman, J. D., et al. 2013, ApJL, 772, L2
Duncan, D. K., Vaughan, A. H., Wilson, O. C., et al. 1991, ApJS, 76, 383
Eastman, J., Gaudi, B. S., & Agol, E. 2013, PASP, 125, 83
Eastman, J. D., Beatty, T. G., Siverd, R. J., et al. 2016, AJ, 151, 45
Foreman-Mackey, D., Hogg, D. W., Lang, D., & Goodman, J. 2013, PASP, 125, 306
Gaia Collaboration, Brown, A. G. A., Vallenari, A., et al. 2016, arXiv:1609.04172
Gillon, M., Pont, F., Demory, B.-O., et al. 2007, A&A, 472, L13
Gregory, S. G., Donati, J.-F., Morin, J., et al. 2012, ApJ, 755, 97
Hansen, B. M. S., & Murray, N. 2013, ApJ, 775, 53
Hartman, J. D., Bakos, G. Á, Buchhave, L. A., et al. 2015, AJ, 150, 197
Hartman, J. D., Bakos, G. Á, Torres, G., et al. 2011, ApJ, 742, 59
Heap, S. R., Lindler, D. J., Lanz, T. M., et al. 2000, ApJ, 539, 435
Hirano, T., Fukui, A., Mann, A. W., et al. 2016, ApJ, 820, 41
Hirano, T., Narita, N., Shporer, A., et al. 2011, PASJ, 63, 531
Høg, E., Fabricius, C., Makarov, V. V., et al. 2000, A&A, 355, L27
Houk, N., & Swift, C. 1999, Michigan Spectral Survey, Vol. 5 (Ann Arbor MI: Dep. Astron., Univ. Michigan), 0
Howell, S. B., Sobeck, C., Haas, M., et al. 2014, PASP, 126, 398
Huang, C., Wu, Y., & Triaud, A. H. M. J. 2016, ApJ, 825, 98
Huber, D., Carter, J. A., Barbieri, M., et al. 2013, Sci, 342, 331
Johnson, M. C., Cochran, W. D., Albrecht, S., et al. 2014, ApJ, 790, 30
Kalas, P., & Jewitt, D. 1995, AJ, 110, 794
Kempton, E. M.-R., Lupu, R. E., Owusu-Asare, A., Slough, P., & Cale, B. 2016, arXiv:1611.03871
Kraft, R. P. 1967, ApJ, 150, 551
Kraft, R. P. 1970, in Spectroscopic Astrophysics: An Assessment of the Contributions of Otto Struve, ed. G. H. Herbig (Berkeley, CA: Univ. California Press), 385
Kreidberg, L., Bean, J. L., Désert, J.-M., et al. 2014, Natur, 505, 69
Kurucz, R. L. 1992, in IAU Symp. 149, The Stellar Populations of Galaxies, ed. B. Barbuy & A. Renzini (Cambridge: Cambridge Univ. Press), 225
Lee, E. J., Chiang, E., & Ormel, C. W. 2014, ApJ, 797, 95
Li, G., & Winn, J. N. 2016, ApJ, 818, 5
Line, M. R., Stevenson, K. B., Bean, J., et al. 2016, AJ, 152, 203
Lissauer, J. J., Marcy, G. W., Rowe, J. F., et al. 2012, ApJ, 750, 112
Lissauer, J. J., Ragozzine, D., Fabrycky, D. C., et al. 2011, ApJS, 197, 8
López-Morales, M., Haywood, R. D., Coughlin, J. L., et al. 2016, AJ, 152, 204
Mann, A. W., Gaidos, E., Mace, G. N., et al. 2016, ApJ, 818, 46
Marino, S., Perez, S., & Casassus, S. 2015, ApJL, 798, L44
Mazeh, T., Perets, H. B., McQuillan, A., & Goldstein, E. S. 2015, ApJ, 801, 3
McLaughlin, D. B. 1924, ApJ, 60, 22
Morton, T. D. 2012, ApJ, 761, 6
Morton, T. D. 2015, VESPA: False Positive Probabilities Calculator, Astrophysics Source Code Library, ascl:1503.011
Morton, T. D., Bryson, S. T., Coughlin, J. L., et al. 2016, ApJ, 822, 86
Nelson, B., & Davis, W. D. 1972, ApJ, 174, 617
Popper, D. M., & Etzel, P. B. 1981, AJ, 86, 102
Quinn, S. N., White, T. R., Latham, D. W., et al. 2015, ApJ, 803, 49
Ricker, G. R., Winn, J. N., Vanderspek, R., et al. 2015, JATIS, 1, 014003
Rodriguez, J. E., Zhou, G., Cargile, P. A., et al. 2017, ApJ, 836, 209
Rossiter, R. A. 1924, ApJ, 60, 15
Sanchis-Ojeda, R., Fabrycky, D. C., Winn, J. N., et al. 2012, Natur, 487, 449
Sanchis-Ojeda, R., & Winn, J. N. 2011, ApJ, 743, 61
Sanchis-Ojeda, R., Winn, J. N., Dai, F., et al. 2015, ApJL, 812, L11
Seager, S., & Mallén-Ornelas, G. 2003, in ASP Conf. Ser. 294, Scientific Frontiers in Research on Extrasolar Planets, ed. D. Deming & S. Seager (San Francisco, CA: ASP), 419
Sing, D. K. 2010, A&A, 510, A21
Sinukoff, E., Howard, A. W., Petigura, E. A., et al. 2016, ApJ, 827, 78
Skrutskie, M. F., Cutri, R. M., Stiening, R., et al. 2006, AJ, 131, 1163
Southworth, J., Maxted, P. F. L., & Smalley, B. 2004, MNRAS, 351, 1277
Sozzetti, A., Torres, G., Charbonneau, D., et al. 2007, ApJ, 664, 1190
Spalding, C., & Batygin, K. 2014, ApJ, 790, 42
Sullivan, P. W., Winn, J. N., Berta-Thompson, Z. K., et al. 2015, ApJ, 809, 77
Torres, G., Andersen, J., & Giménez, A. 2010, A&A Rev., 18, 67
van Saders, J. L., & Pinsonneault, M. H. 2013, ApJ, 776, 67
Vanderburg, A., Becker, J. C., Kristiansen, M. H., et al. 2016a, ApJL, 827, L10
Vanderburg, A., Bieryla, A., Duev, D. A., et al. 2016b, ApJL, 829, L9
Vanderburg, A., & Johnson, J. A. 2014, PASP, 126, 948
Vanderburg, A., Latham, D. W., Buchhave, L. A., et al. 2016c, ApJS, 222, 14
Wang, J., Xie, J.-W., Barclay, T., & Fischer, D. A. 2014, ApJ, 783, 4
Weiss, L. M., & Marcy, G. W. 2014, ApJL, 783, L6
Winn, J. N., Fabrycky, D., Albrecht, S., & Johnson, J. A. 2010, ApJL, 718, L145
Wright, E. L., Eisenhardt, P. R. M., Mainzer, A. K., et al. 2010, AJ, 140 1868
Yi, S., Demarque, P., Kim, Y.-C., et al. 2001, ApJS, 136, 417
Zhou, G., Rodriguez, J. E., Collins, K. A., et al. 2016, AJ, 152, 136